UNIVERSITY OF NOVA GORICA

SCHOOL OF APPLIED SCIENCES

MEASUREMENT OF DAILY VARIATION CYCLE OF PLANETARY BOUNDARY LAYER PROPERTIES

DIPLOMA THESIS

Ivana Vasilevska

ADVISER: prof.dr. Samo Stanič

Ajdovščina, 2012

UNIVERZA V NOVI GORICI

FAKULTETA ZA APLIKATIVNO NARAVOSLOVJE

MERITEV DNEVNEGA CIKLA VARIACIJ LASTNOSTI PLANETARNE MEJNE PLASTI

DIPLOMSKO DELO

Ivana Vasilevska

MENTOR: prof.dr. Samo Stanič

Ajdovščina, 2012

ACKNWNOLEDGMENTS

I wish to express my sincere gratitude to prof. dr. Samo Stanič for his help, advices, and guidance in my work, as well as Fei Gao and Tingyao He for all the help, advices and support. Many thanks to prof. dr. Martin O'Loughlin for his help with Octave and Marko Vučković for his help with Matlab.

I would like to express my gratitude to my parents, my husband, my brother and his wife, for their support, understanding, and love.

Abstract

The aim of the diploma thesis was to investigate the variation of daily aerosol concentrations in Nova Gorica. A measuring campaign using a mobile lidar operating at the wavelength of 1064 nm was performed on 14 January 2012 to investigate the concentration of urban aerosols. Measurements were performed for the whole day, from 06:00 to 22:00 CET. From the collected data, extinction coefficient was calculated using Klett method and presented as time-series of Time-Height-Indicator profiles. Daily aerosols concentration cycles were clearly visible with a peak in aerosol concentration at around 19:00 CET at the height of 0.6 km. In addition, the retrieved extinction coefficient was compared to concentrations of PM_{10} particles, NO_x gases and other meteorological data that were continuously monitored by the Slovenian Environment Agency 3 km away from the lidar site. We found a linear correlation between atmospheric extinction coefficient, obtained from the lidar measurements and both PM_{10} concentrations and NO_x, with a correlation coefficient of 0.34 and 0.66, respectively. In order to identify the sources of the aerosols and their trajectories, we used DREAM model and HYSPLIT model to model their arrival paths. The results indicate no presence of Saharan dust as the air masses over Nova Gorica were through the day coming from the north and north-west. The aerosols observed were found to be of local origin.

Keywords: atmospheric boundary layer, aerosols, lidar

Povzetek

Planetarna mejna plast je najnižji del atmosfere in se dviga od površja do višine 1-2 km, v kateri prihaja do izmenjave toplote in snovi z zemeljskim površjem. Povečani izpusti toplogrednih plinov in aerosolov v planetarno mejno plast znižujejo kvaliteto življenjskih pogojev in so lahko v ekstremnih razmerah celo neposredno nevarni za človekovo zdravje, zato redno potekajo okoljske meritve koncentracij polutantov v ozračju. Poleg neposrednega vpliva na ljudi povečane vsebnosti le-teh v ozračju spreminjajo tudi energijsko bilanco zemeljskega površja in s tem vplivajo na vreme in na podnebje. Nova Gorica se nahaja na področju, ki je pred vetrom s severa dobro zaščiteno z lokalnim hribovjem, z zahoda z Goriškimi Brdi in z jugovzhoda s Kraško planoto. Zaradi omenjene konfiguracije terena lahko pričakujemo, da bodo lokalni izvori aerosolov imeli močan vpliv na kvaliteto zraka v Novi Gorici. Koncentracije aerosolov praviloma merimo s pomočjo meteoroloških postaj, ki pa nam omogočajo le točkovne meritve nekaj metrov nad površjem. V diplomskem delu predstavljamo raziskavo variacije dnevnih koncentracij aerosolov v troposferi nad Novi Gorico z uporabo mobilnega lidarja. Mobilni lidar, ki je bil na Univerzi v Novi Gorici razvit leta 2007, sestavljata bi-aksialno nameščena oddajnik in sprejemnik svetlobe ter analogno-digitalni pretvornik in računalnik za shranjevanje in obdelavo podatkov. Kot oddajnik smo uporabili Nd:YAG laser, ki oddaja 8 ns dolge svetlobne pulze pri valovni dolžini 1064 nm s frekvenco 10 Hz ter energijo 40 mJ/pulz. Laserska svetloba se v atmosferi na delcih in molekulah siplje v vse smeri. Za sprejemnik povratno sipane svetlobe smo uporabili teleskop s premerom 300 mm, svetlobni signal pa smo pretvorili v električnega z plazovno fotodiodo (APD), ga pretvorili v digitalno obliko s pomočjo analogno-digitalnega pretvornika in shranili z računalnikom.

Eksperimentalni del diplomske naloge temelji na vertikalnih meritvah povratnega sipanja na aerosolih v atmosferi, izvedenih 14 januarja 2012. Meritve so potekale od 06:00 do 22:00 CET v 5 minutnih časovnih intervalih. Iz lidarskih signalov smo koeficient atmosferske ekstinkcije (α) izluščili s Klettovo metodo. Za razumevanje dinamike sprememb v atmosferi smo višinski profil koeficienta ekstinkcije prikazali kot časovno zaporedje. Iz rezultatov lahko zaključimo, da so se koncentracije aerosolov 14.1.2012 v Novi Gorici začele večati v popoldanskem času in so dosegle maksimalne dnevne vrednosti okoli 19:00 CET. Opazili smo, da koeficient atmosferske ekstinkcije z višino pada, maksimum ($\alpha = 0.07\ km^{-1}$) pa ima na višini okoli 0.6 km, takoj ob vstopu v območje popolnega prekrivanja laserskega žarka in vidnega polja teleskopa. Rezultate lidarskih meritev smo primerjali z meritvami talne meteorološke postaje Agencije za Okolje v Novi Gorici, ki poleg standardnih meteoroloških količin meri tudi koncentracijo delcev z dimenzijami manjšimi od 10μm (PM_{10}) in koncentracije dušikovih oksidov (NO_x) v atmosferi. Ugotovili smo, da je korelacija med koeficientom

atmosferske ekstinkcije ter koncentracijami PM_{10} oziroma NO_x linearna, s korelacijskima koeficientoma 0.66 in 0.34.

Da bi potrdili, da so bile izmerjene koncentracije aerosolov res rezultat lokalnih izpustov, smo izvor zračnih mas nad Novo Gorico modelirali z modelom za opis transporta zračnih mas HYSPLIT. Transportne trajektorije smo izračunali za tri različne višine (500 m, 1500 m in 3000 m) zračnih mas nad Novo Gorico v času meritev za časovni interval do 96 ur pred samo meritvijo s časovno ločljivostjo 6 ur. Ugotovili smo, da so med meritvijo zračne mase prihajale s severa in severozahoda, da so izvirale s področja severnega Atlantika in da so po vsej verjetnosti nosile pretežno aerosole morskega izvora. Z modelom DREAM smo dodatno preverili morebitno vsebnost Saharskega peska nad Novo Gorico v času lidarskih meritev, ki za to obdobje prisotnosti teh aerosolov ne napoveduje. Iz rezultatov lidarskih in okoljskih meritev ter modeliranja transporta zračnih mas lahko zaključimo, da so bile izmerjene povišane koncentracije aerosolov rezultat lokalnih izvorov onesnaženja.

Ključne besede: planetarna mejna plast, aerosol, lidar

To my daughter

Contents

1. INTRODUCTION

Atmospheric boundary layer (ABL) is the lowest part of the atmosphere, in which there is an exchange of heat and substance of the Earth's surface. Increased emissions of the aerosols in the ABL decrease the quality of living conditions. Being part of the atmosphere, aerosols have a big impact on human health, and on climate, by changing the amount of solar energy [1]. With development of remote sensing techniques, lidar has proven to be a powerful tool for the study of the ABL structure [2]. In this chapter we present the structure of the Earth's atmosphere, the properties of the aerosols and propagation of light through the atmosphere.

1.1 Structure of the Earth's atmosphere

The atmosphere is a mixture of gases, which surround the Earth, such are nitrogen (78%), oxygen (21%) and other gases (1%) like carbon dioxide (CO_2), methane (CH_4), ozone (O_3) and water vapor. The atmosphere is divided into five main layers. They are, from the top to the bottom, the exosphere, the thermosphere, the mesosphere, the stratosphere, and the troposphere (Fig. 1). We live in the troposphere, the layer from the surface up to 10 km. The gases in this region are mainly oxygen (20%) and nitrogen (78%). All weather occurs in this layer and it contains 99% of water vapor and aerosols, such as dust particles. Because of the gravity, the properties of the air, such as atmospheric pressure and density are higher near the Earth's surface and decrease exponentially with altitude. The troposphere can be divided into two parts: the bottom of the troposphere, 1-2 km above the Earth's surface and the free troposphere. The bottom of the troposphere is called ABL, and its behavior is directly influenced by interaction with the surface [3].

1.2 Aerosols

Aerosols are solid or liquid particles floating in the atmosphere. They range in sizes from 0.01 μm to several tens of μm (Fig. 2). There are thousands of aerosols in each cubic centimeter of air. Concentrations of aerosols are bigger in the ABL, than they are in the free troposphere. Some of them are natural and others are anthropogenic, that are produced by humans. The natural sources of aerosols are pollen from the

flowers, dust from dry regions, and particles from eruption of volcanoes or forest fires and salt from the oceans. The man-made (anthropogenic) sources of aerosols are air pollution from the factories that burn fossil fuels, from auto emissions and from the power plants.

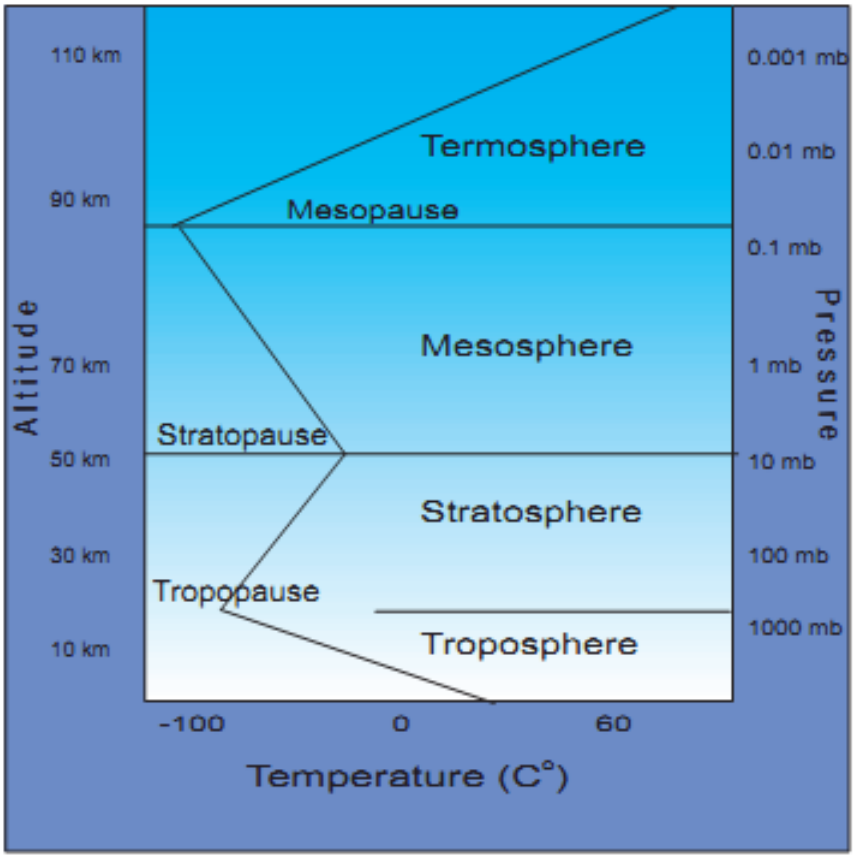

Figure 1: The schematic view of atmospheric layers. The lowest layer is troposphere, in which we live. The temperature decreases with height. The tropopause is boundary layer between troposphere and stratosphere. Stratosphere is a layer above the troposphere, in which temperature is increasing with height. A maximum in stratospheric temperature occurs in stratopause, which is the boundary between stratosphere in mesosphere. Mesosphere is above the stratosphere. The temperature decreases with height. Boundary between mesosphere and thermosphere is mesopause, in which there is a minimum in temperature profile [4].

The aerosols are dangerous for human health and also have an impact on the climate. Aerosols in the atmosphere change the amount of solar energy. They have a "direct" cooling effect by scattering and absorbing the solar radiation. The aerosols also have the "indirect" effect on climate by changing the cloud microphysical and radioactive properties, lifetime, amount and morphology of clouds which reflect the energy from the sun back out to space [5]. For example, sea salt particles reflect the energy from the sun back to the space. Black carbon particles from fossil fuels absorb the sunlight that reaches the surface energy.

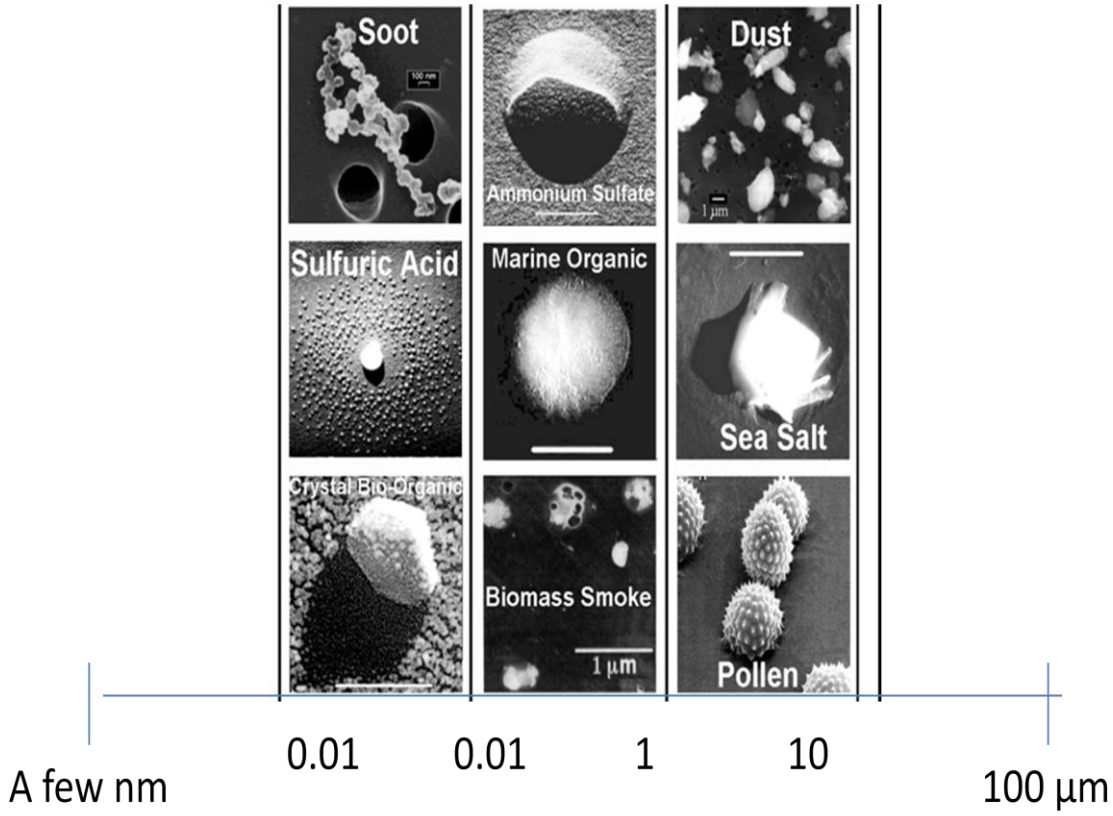

Figure 2: Sizes of the aerosols: from 0.01 µm for soot, sulfuric acid to several tens of µm for dust, sea salt and pollen particles [5].

1.3 Light propagation through the atmosphere

When light goes through the medium, it is scattered and/or absorbed. A photon of light is scattered when it is received by the particle and re-radiated at the same wave-

length [4]. Particles larger than the wavelength of the incident light can scatter light through three processes: diffraction, phase shift and refraction. Particle can also absorb photons and convert them to internal thermal energy. Scattering can be elastic or inelastic. The wavelength of the incident radiation remains the same after the process of elastic scattering. There are three different types of elastic scattering: Rayleigh, Mie and non-selective scattering. In inelastic scattering, the wavelength of the incident radiation changes and this includes resonant scattering, fluorescence and Raman scattering.

1.3.1 Rayleigh scattering

Rayleigh (molecular) scattering [6, 7] is elastic scattering on atmospheric molecules and small particles, which are much smaller in size compared to the wavelength of incident radiation. This type of scattering is wavelength dependent. If we ignore depolarization effects and the adjustments for temperature and pressure, the molecular angular scattering coefficient at wavelength λ in the direction θ relative to the direction of the incident light can be written as

$$\beta_{\mathrm{m}}(\theta) = \frac{\pi^2 (n^2 - 1)^2 N_{\mathrm{m}}}{2 N_{\mathrm{s}}^2 \lambda^4} (1 + \cos^2 \theta), \tag{1}$$

where n is the real part of the index of refraction, N_{m} is number of molecules per unit volume (number density) and N_{s} is the number density of molecules at standard conditions (N_{s}=2.547·10^{19} cm^{-3} at T=288.15 K and P_{s}=101.325 kPa). The term (1+cos$^2\theta$) is Rayleigh phase function under the assumption of isotropic distribution of air molecules [7]. Total molecular scattering coefficient can be obtained as an integral over the entire solid angle,

$$\beta_{\mathrm{m}}^{\mathrm{tot}} = \int_{\phi=0}^{2\pi} \int_{\theta=0}^{\pi} \beta_{\mathrm{m}}(\theta) \sin\theta \, \mathrm{d}\theta \, \mathrm{d}\phi, \tag{2}$$

which after substituting $\beta_{\mathrm{m}}(\theta)$ from Eq. (1) gives

$$\beta_{\mathrm{m}}^{\mathrm{tot}} = \frac{8\pi^3 (n^2 - 1)^2 N_{\mathrm{m}}}{3 N_{\mathrm{s}}^2 \lambda^4}. \tag{3}$$

For the case of lidar, the molecular backscattering coefficient can be obtained as

$$\beta_{\mathrm{m}} = \beta_{\mathrm{m}}(\theta = 0^{\circ}) = \frac{\pi^2 (n^2 - 1)^2 N_{\mathrm{m}}}{N_{\mathrm{s}}^2 \lambda^4} \tag{4}$$

and has units [$m^{-1}sr^{-1}$]. It stands for the ability of the atmosphere to scatter light back into the direction from which it comes [6] and is inversely proportional to the fourth power of the wavelength of incident light. The equation implies that atmospheric gases scatter much more light in the ultraviolet part than in the infrared part of the spectrum.

In scattering theory, the term "cross section" is defined as the amount of scattering on a single molecule

$$\sigma_{\mathrm{m}} = \frac{\beta_{\mathrm{m}}^{\mathrm{tot}}}{N_{\mathrm{m}}}, \tag{5}$$

and has units [m^2sr^{-1}].

For Rayleigh scattering, the scattering cross section σ_m can be written as

$$\sigma_{\mathrm{m}} = \frac{8\pi^3 (n^2 - 1)^2}{3 N_{\mathrm{s}}^2 \lambda^4} \tag{6}$$

by substituting Eq. (4) into Eq. (5).

1.3.2 Mie scattering

Mie scattering [6, 7] occurs when the particles causing the scattering are larger in size than the incident wavelength of light. This scattering process is called "Mie scattering", developed by Gustav Mie (1908), who first provided a quantitative theoretical explanation [3, 6]. The intensity of light scattering by particulates depends on geometric size and shape of the scattering particle, the refractive index of the particle, the wavelength of the incident light, and the particulate number density. In the following description, it is assumed that scatters are spherical, incident light is spectrally narrow, and multiple scattering is negligible and can be ignored.

1.3.3 Monodisperse scattering approximation

For case of the monodisperse scattering approximation, the scattering volume under consideration is assumed to be filled uniformly by particles on the same size and composition. These particulates have the same scattering properties. Similar to molecular scattering, the total particle scattering is

$$\beta_{\mathrm{p}} = N_{\mathrm{p}}\sigma_{\mathrm{p}}, \tag{7}$$

where N_{p} is the particle number density and σ_{p} is the single particle cross section. In scattering theory, two additional parameters are defined: scattering efficiency and size parameter. Scattering efficiency Q_{sc} is defined as the ratio of particulate cross section σ_{p} to the geometric cross-sectional area of the scattering particle,

$$Q_{\mathrm{sc}} = \frac{\sigma_{\mathrm{p}}}{\pi\rho^2}, \tag{8}$$

where ρ is the particle radius. The size parameter φ is defined as

$$\varphi = \frac{2\pi\rho}{\lambda}, \tag{9}$$

where λ is the wavelength of the incident light. By substituting the cross section σ_{m} from Eq. (8), the total particulate scattering coefficient β_{p} can be written as

$$\beta_{\mathrm{p}} = N_{\mathrm{p}}\pi\rho^2 Q_{\mathrm{sc}}. \tag{10}$$

The dependence of the scattering efficiency Q_{sc} on size parameter φ for four different indexes of refraction, m=1.10, 1.33, 1.50 and 1.90 is shown in Fig. 3. We can see that if the size parameter φ is small (φ<0.5), the scattering efficiency factor is also small. As the size parameter increases, the scattering efficiency factor increases, reaching the maximum values of Q_{sc}. When the size parameter φ > 30, the scattering efficiency factor decreases and oscillates about an asymptotic value of Q_{sc}=2. In this case, the scattering does not depend on the wavelength of incident light.

Depending on particles, scattering can be separated into three specific types. When φ<<1, the scattering is similar to the Rayleigh scattering and is characterized by small particles, found in clear atmosphere. The region where φ>>40-50 characterizes scat-

tering by large particles, found in heavy fogs and clouds. The intermediate type where $1<\varphi<25$, characterizes scattering by particles that are found in the lower troposphere.

The fact that Q_{sc} converges to 2 at large values of φ is due to the details of refractive scattering and can be interpreted as interaction of a scattering particle with incident light over an area twice as large as its physical cross-section [3].

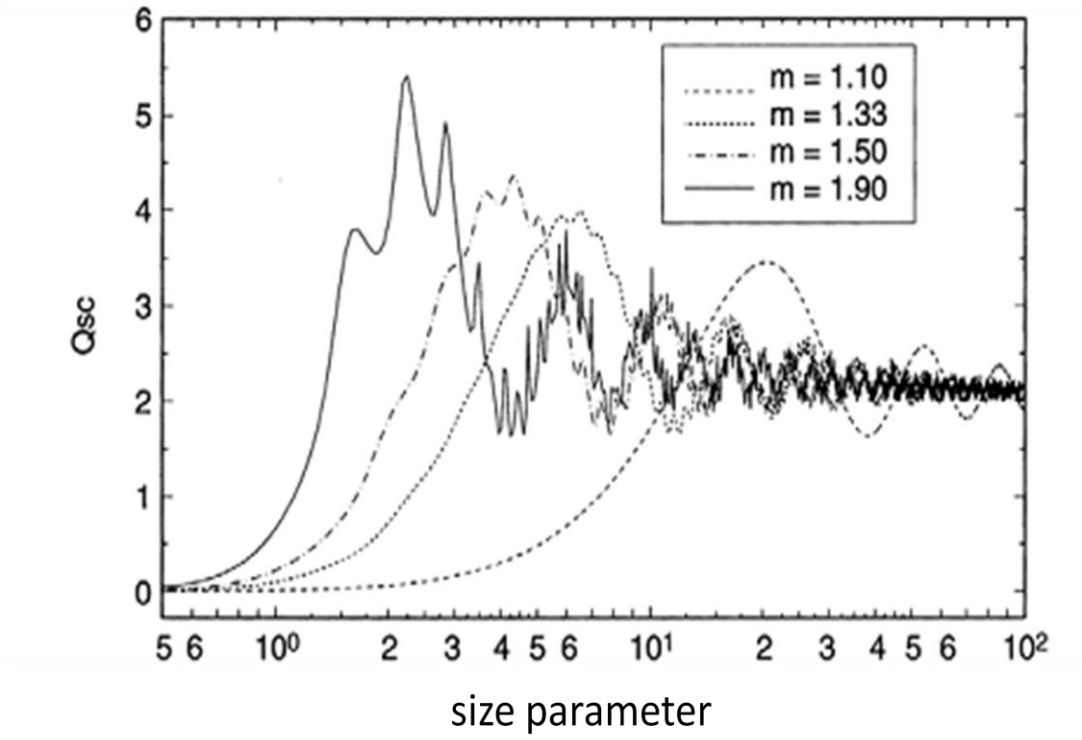

Figure 3: The dependence of particulate scattering factor Q_{sc} on the size parameter φ for different indexes of refraction without absorption [3].

1.3.4 Polydisperse scattering approximation

In the real atmosphere, there are particulates that differ in composition and geometric size, so assumption of uniformity is not practical. The total number of particulates in a unit volume of air is defined as sum of all scatterers in the volume,

$$N = \sum_{i=1}^{k} N(\rho_i), \tag{11}$$

where $N(\rho_i)$ is the number of particulates with radius ρ_i. The total scattering coefficient is defined as sum of the appropriate constituents,

$$\beta_{\mathrm{p}} = \sum_{i=1}^{k} N(\rho_i)\pi\rho_i^2 Q_{\mathrm{sc},i}. \tag{12}$$

The last type of elastic scattering is non-selective scattering, which occurs in the troposphere where the radius of the particles is much larger than the incident radiation wavelength. An example of non-selective scattering is the scattering of sun light by atmospheric constituents such as large aerosols, cloud droplets or ice crystals [4]. This type of scattering is not wavelength dependent and is the cause of hazes.

2. EXPERIMENTAL SETUP

Atmospheric aerosols including dust, smoke and clouds which are mainly present in troposphere play an important role in the Earth's climate system, in particular regarding global warming. To better understand the effects of aerosols on the climate, new observational instruments and techniques are being developed, one of them is laser-based remote sensing (lidar). Lidar [8-11] is a modern remote-sensing tool for the study of optical properties of the atmospheric aerosols. The acronym LIDAR (**Li**ght **D**etection **A**nd **R**anging) first time was introduced by Middleton and Spilhaus in 1953. The development of the Lidar technology started with invention of the laser in 1960 and the giant pulse or Q-switched laser in 1962 [6]. Using a lidar, it is possible to detect spatial distribution of aerosols and clouds [8]. University of Nova Gorica has two operational lidars, one stationary at Otlica, and one scanning mobile lidar system. In this chapter, we describe the basic lidar setup, and the configuration of the scanning mobile lidar system at University of Nova Gorica.

2.1 Lidar setup

General setup of a lidar system is shown in Fig. 4. Lidar transmits short pulses of laser light directed at a certain elevation angle into the atmosphere. Laser beam loses light to scattering as it travels. The backscattered light is collected by the reflective and refractive optics and transferred to photo-detectors which can be either photomultiplier tubes (PMT) for ultraviolet (UV) and visible light or avalanche photodiodes (APDs) for infrared (IR) light. Analog signals from the photo-detectors are transformed into digital ones, more suitable for data analysis, using a transient recorder. Digital data is stored by data acquisition (DAQ) software. Because the light takes longer to return from larger distances, the time delay of the return pulses can be converted into the corresponding distance between the atmospheric scatterer and the lidar device. From the intensity of backscattered light, the density of the scatterers can be obtained. The end result is a profile of atmospheric scattering versus distance. Analysis of this signal can yield information about the presence, location and optical properties of the aerosols in the atmosphere.

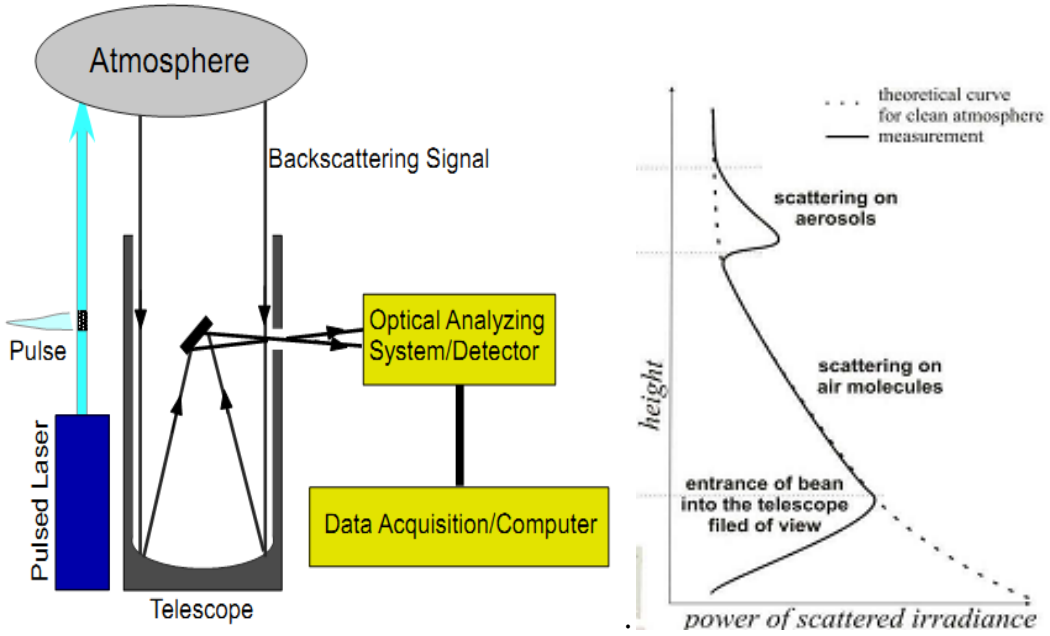

Figure 4: Shematic diagram of a typical lidar setup and its lidar returns. Left: A basic LIDAR system is comprised of a transmitting optics (laser), receiving optics (telescope), detection system and equipment for acquisition of data [7]. Laser pulses are emitted into the atmosphere, interacting with both the gas, molecules and the aerosols present. Backscattered light is collected by the telescope. The return signals are detected by the detector, and transformed into digital information using digitizer. Electrical signal is analyzed by DAQ computer. Right: The analog signal represents the amount of backscattered light which is decreasing with the distance from the lidar [4].

2.2 Configuration of the mobile lidar system at University of Nova Gorica

The scanning mobile lidar, which was developed in 2007 at the University of Nova Gorica, was designed primarily for studies of the lower troposphere. It provides automatic scanning capability in both azimuth and elevation angles with angular resolution of 0.1° (Fig. 5) and can operate in both day-time and night-time conditions [8, 10]. Its schematic diagram is shown in Fig. 6.

2.2.1 Transmitter

As a transmitter, we used the Nd:YAG laser (Quantel Big Sky CFR400) laser (Fig. 7). This particular laser is capable of simultaneous emission of light pulses at 1064 nm (infrared), 532 nm (green) and 266 nm (ultraviolet light), however only the 1064 nm light was used in our experiment. IR light is namely most suitable for aerosol studies because the molecular backscattering at these wavelengths is negligible. The 1064 nm and 266 nm beams overlap as they exit the laser (Fig. 8) and have a divergence angle of 0.7 mrad. Pulse energy at the wavelength of 1064 nm and pulse width of 8 ns is 40 mJ. Pulse repetition frequency is 10 Hz.

Figure 5: Servo motors and transmission systems for movement lidar. Azimuth and elevation angles can be set with 0.1° precision.

2.2.2 Receiver

The receiver and the transmitter are configured bi-axially. Backscattered light is collected by Newtonian telescope, which is a product of Guan Sheng Optical Company (Fig. 9). Inside, there are two mirrors. The one is a parabolic mirror, with a diameter of 302 mm and a focal length of 1520 mm, which collects the backscattered light from the atmosphere. The other mirror is a reflector mirror to redirects light into detecting system. At the focus of the telescope an adjustable iris was placed to reduce its field of view. After this iris, light is re-collimated and split into three channels using dichroic beam splitters and partial reflection mirrors.

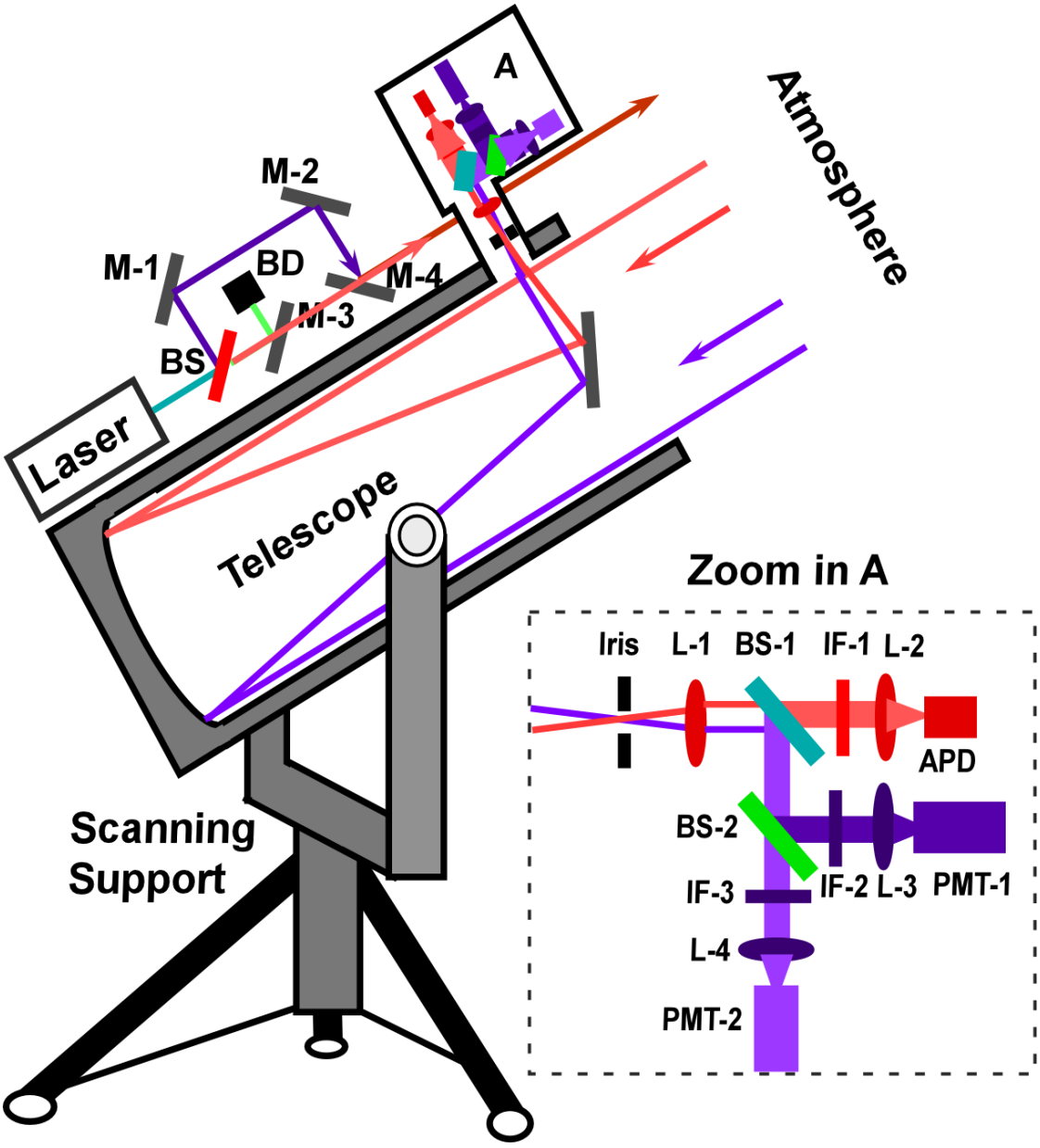

Figure 6: Schematic diagram of the optical components of the scanning mobile lidar. A detailed description of the spectroscopic filter is shown as an enlargement. BD: Beam Dump, BS: Beam Splitter, IF: Interference Filter, PMT: Photomultiplier Tube, APD: Avalanche Photodiode [8].

Figure 7: Quantel Big Sky laser used in the experiment. Top photograph shows its front panel with controls for pulse energy and frequency and the bottom photograph the laser head.

2.2.3 Detection system

Dichroic beam splitters made by SLS Optics Limited were applied to divide elastic scattering (at 1064 nm and 266 nm) and induced fluorescence (UV). The first dichroic beam splitter in the receiver separates UV from IR light. Ultraviolet light is divided once more with the second dichroic beam splitter, where induced fluorescence is separated from elastic scattering (Fig. 5). Return signals are detected by Hamamatsu R7400 photomultiplier tubes (PMT) for 266 nm and 295 nm channels and EG&G C30954/5E Avalanche photodiode (APD) for the 1064 nm channel.

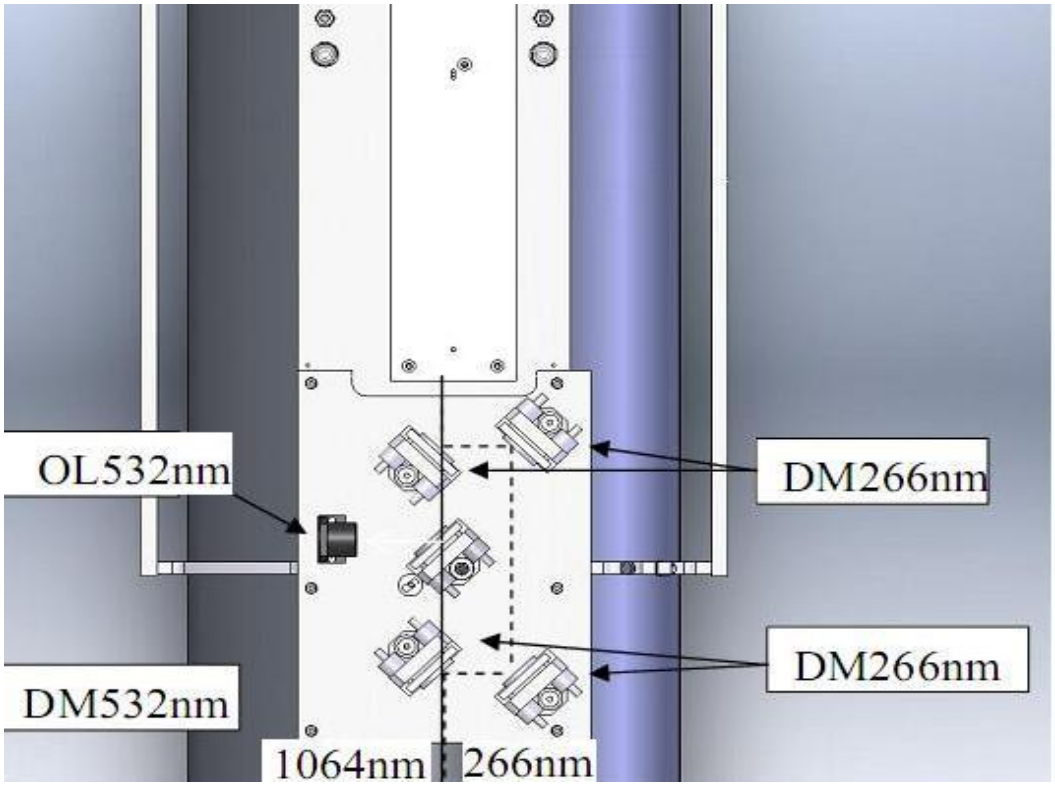

Figure 8: Optical components of the transmitter system. Mirrors redirect laser light into desired direction, where the infrared (1064 nm) and ultraviolet (266 nm) beams overlap as they exit the system.

2.2.4 Data acquisition

Analog electrical signals received from the detectors are transformed into digital information using a TR40-160 Licel transient recorder (Fig. 10) with 12-bit resolution at 40 MHz sampling rate in combination with C++ (Linux) based data acquisition software, developed at the University of Nova Gorica. These digitization parameters yield a range resolution of 3.75 m. The transient recorder is connected to a Linux based data acquisition (DAQ) computer via an Ethernet link.

Figure 9: Detection system of the lidar. Return signals are detected by the photomultiplier tubes (PMT) for 266 nm and 295 nm channels and Avalanche photodiode (APD) for the 1064 nm channel. Receiver of the backscattered light is Newtonian telescope.

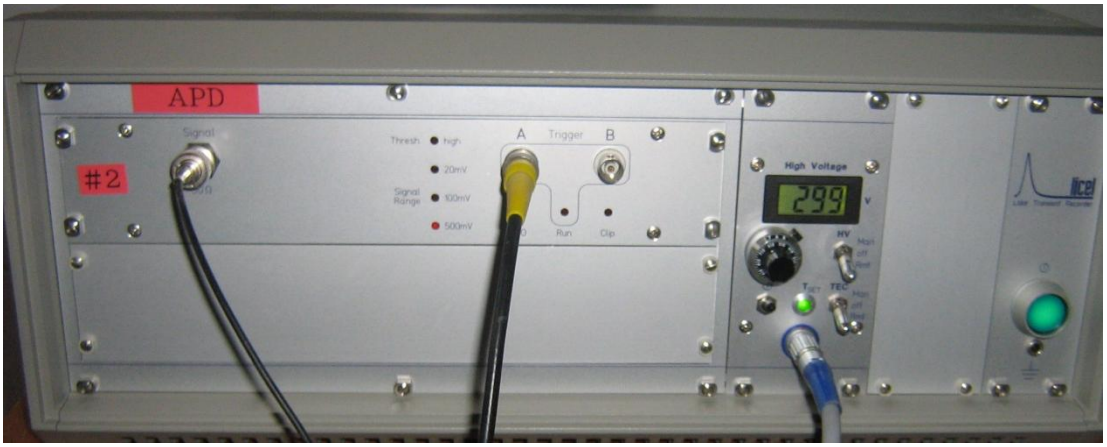

Figure 10: Licel transient recorder TR40-160 with a 12-bit resolution at 40 MHz sampling rate and 16k trace length in analog mode combined with 250 MHz discriminator in photon-counting mode for transforming the analog signal from detector into digital information. The module also includes high voltage control for the detector (PMT or APD).

3. RETRIEVAL TECHNIQUE

The detected lidar signal is described by the single-scattering lidar equation:

$$P(r) = P_0 k \frac{c\tau_0}{2} A \frac{\beta(r)}{r^2} T^2(r). \quad (13)$$

P(r) is instantaneous received backscattered power at time *t* from distance *r*, P_0 transmitted laser power at time t_0, *k* is system efficiency, τ pulse duration, *c* the velocity of light, *A* the effective receiver area of the detector, which is responsible for the collection of the backscattered light.

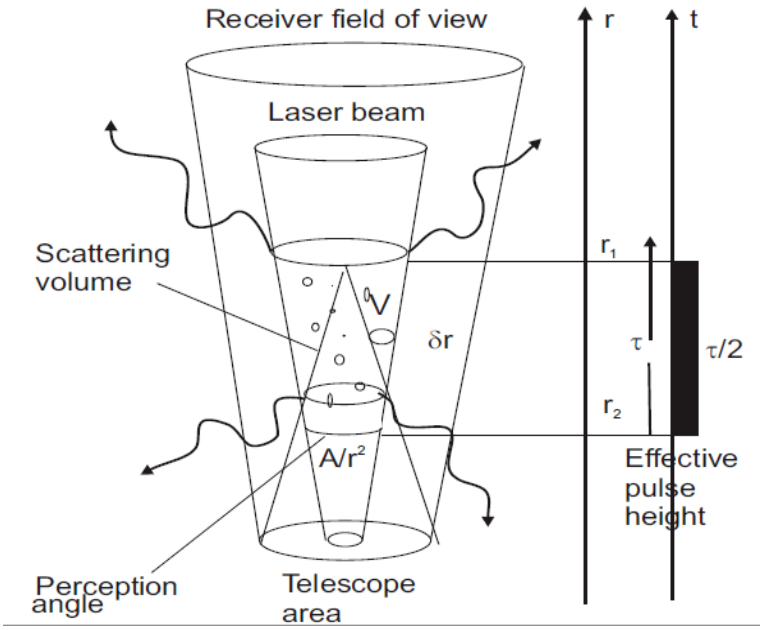

Figure 11: Illustration of the lidar equation. When the lidar signal is detected at any instant time *t* after the leading edge of the pulse was emitted, backscattered light from the leading edge of the pulse comes from the distance $r_1=ct/2$. At the same time, light produced by trailing edge arrives from distance $r_2=c\ (t-\tau)/2$. Thus, $\delta r=r_1- r_2=c\tau/2$ is the length of the volume from which backscattered light is received at any instant time and is called "effective (spatial) pulse length". *A* is the area of the primary receiver optics responsible for collection of backscattered light [4, 6].

Equation (13) shows that the return signal changes dramatically with the distance. The quadratic decrease of the signal intensity with distance is due to the fact that receiver telescope area makes a part of a sphere's surface with radius r that encloses the scattering volume. The solid angle $A/4\pi r^2$ gives the perception angle of the lidar for light scattered at distance r [4]. These processes are graphically presented in Fig. 11. The term $\beta(r)$ is the backscattering coefficient, which is used to determine the strength of the signal. It describes how much light is scattered into backward direction, i.e. toward the lidar receiver.

In the atmosphere, the laser light is scattered by air molecules and particle matter, $\beta(r)$ can be written as

$$\beta(r,\lambda) = \beta_{\text{mol}}(r,\lambda) + \beta_{\text{aer}}(r,\lambda). \tag{14}$$

$T(r)$ is transmission term and describes how much light gets lost on the way from the lidar to distance r and back. The transmission term can take values between 0 and 1 and it is according to "Bouguer-Lambert law" described as a negative exponential as

$$T(r) = e^{-\tau(r)} = \exp(-\int_0^r \alpha(r)\mathrm{d}r), \tag{15}$$

where $\tau(r)$ is optical depth, and $\alpha(r)$ is attenuation (extinction) coefficient.

The integral considers the path from the lidar to distance r. The factor 2, which appears in Eq. (13), is for two-way transmission path, since the photons have to travel to distance r and then back to the lidar. Extinction coefficient, like the backscattering coefficient, is described as the product of number concentration and extinction cross-section, and has a unit [m^{-1}]. Extinction can occur because of scattering and absorption of light by molecules and particles:

$$\alpha(r,\lambda) = \alpha_{\text{mol,sca}}(r,\lambda) + \alpha_{\text{mol,abs}}(r,\lambda) + \alpha_{\text{aer,sca}}(r,\lambda) + \alpha_{\text{aer,abs}}(r,\lambda), \tag{16}$$

where the indices "sca" and "abs" stand for scattering and absorption.

Backscattering and extinction coefficients depend on the wavelength of the laser light. The wavelength dependence is determined by the size, the refractive index, and the shape of the scattering particles [6].

Introducing a new variable $S(r) \equiv \ln\left[r^2 P(r)\right]$, with $S=S(r)$, $S_0=S_0(r)$ and r_0 a given constant reference range, Eq. (13) can be written as [12],

$$S - S_0 = \ln\frac{\beta}{\beta_0} - 2\int_{r_0}^{r} \alpha \mathrm{d}r, \tag{17}$$

where $\beta_0=\beta(r_0)$.

The differential equation corresponding to Eq. (17) is

$$\frac{\mathrm{d}S}{\mathrm{d}r} = \frac{1}{\beta}\frac{\mathrm{d}\beta}{\mathrm{d}r} - 2\alpha \ . \tag{18}$$

Solution of this equation requires an assumption of a relationship between $\beta(r)$ and $\alpha(r)$. For homogeneous atmosphere, the term $\frac{\mathrm{d}\beta}{\mathrm{d}r} = 0$, so extinction coefficient can be expressed in terms of the signal slope

$$\alpha_{\mathrm{hom}} = -\frac{1}{2}\frac{\mathrm{d}S}{\mathrm{d}r}. \tag{19}$$

A plot of $S(r)$ versus range r would be a straight line whose slope is -2α [13].

The solution of the Lidar equation, Eq. (19), can not be applied for inhomogeneous atmosphere. For solving Lidar equation, a relationship between backscatter $\beta(r)$ and attenuation coefficient $\alpha(r)$ must be introduced.

$\beta(r)$ and $\alpha(r)$ can be related according to a power law of the form

$$\beta(r) = A\alpha(r)^k, \tag{20}$$

where k depends on the lidar wavelength and properties of the aerosols. Typical values of the exponent are in the interval $0.67 \le k \le 1.0$.

Now, with the power law from Eq. (20), Eq. (18) can be rewritten as

$$\frac{\mathrm{d}S}{\mathrm{d}r} = \frac{k}{\alpha}\frac{\mathrm{d}\alpha}{\mathrm{d}r} - 2\alpha \ . \tag{21}$$

This type of equation is nonlinear, called Bernoulli equation, which can be transformed into first order linear form by introducing a new unknown equal to the reciprocal of the original. The solution of the Eq. (18) can be written as

$$\alpha(r)=\frac{\exp\left[\left(S-S_{\mathrm{m}}\right)/k\right]}{\frac{1}{\alpha_{\mathrm{m}}}+\frac{2}{k}\int_{r}^{r_m}\exp\left[\left(S-S_{\mathrm{m}}\right)/k\right]\mathrm{d}r}, \tag{22}$$

where $S_{\mathrm{m}}=S(r_{\mathrm{m}})$, and $\alpha_{\mathrm{m}}=\alpha(r_{\mathrm{m}})$.

This method for the retrieval of atmospheric optical variables from Mie lidar return signal is called the Klett method [12].

4. MEASUREMENTS OF DAILY VARIATIONS OF AEROSOL CONTENT

On 14 January 2012 we performed a measurement campaign, to investigate the variation of daily aerosol concentrations over Nova Gorica. The lidar was set up at Rožna dolina (45.96° N, 13.64° E, 107 a.s.l.) in vertical direction. Figure 12 shows the operating condition of the lidar system. The measurements were performed from 06:00 CET to 22:00 CET (Central European Time), in 5 minute intervals. The atmospheric conditions were stable. During the measurements the sky was quite clear, except for some clouds around noon. With these measurements we investigated the variation of aerosol concentrations during the day. Data analysis and graphs were done in Matlab software, version 7.0.1.24704 (R14), 2004.

The lidar return signal was described by the Lidar equation (Eq. 13). From the data that we collect, raw data was normalized to the laser energy, and the flat baseline of each return, which is proportional to the intensity of background noise, was subtracted. Background noise was defined as an average of data points sampled at the far end of the trace, and it can be airglow, starlight, stray moonlight and electronic noise from detector and digitizer. Then, each lidar return was corrected to logarithm of range-squared signal. Time series of logarithm of range-squared signal profiles are present in Fig. 13. From the morning profiles, we can see that atmospheric conditions were stable, until noon, when there was cloud appearing at 13:00 CET at height of 3 – 4 km. In the afternoon and evening, more aerosol layers were appearing within the ABL. The maximum aerosol concentration was at 19:00 CET at a height of 0.6 km. From the Time-Height Indicators for logarithm of range-squared signal (Fig. 14), we can see that in the morning the sky was clear and atmosphere was stable. The aerosol content was low. At the noon around 13:00 CET at height of 3 - 4 km we detected a little cloud, which has gone quickly. The atmosphere was quite stable up to 17:00 CET. After that, the high aerosol concentrations were present in the afternoon, from local-ground sources with maximum concentration at 19:00 CET at the height of 0.6 km, which can be related to human activities.

Figure 12: Working condition of the lidar system for vertical measurements at University of Nova Gorica on 14 January 2012. Data was taken in 5 minutes intervals from 06:00 to 22:00 CET. Solid state Nd:YAG (Quantel Big Sky) laser was used, operating at 1064 nm wavelength, providing 40 mJ pulse energy and 8 ns pulse width with repetition rate 10 Hz. Backscattered light was collected by the Newtonian telescope with a diameter of 302 mm. The signal was detected by EG&G C30954/5E Avalanche photodiode (APD) and digitized using TR40-160 Licel transient recorder with 12-bit resolution at 40 MHz sampling rate. Digital data was retrieved through an Ethernet link and stored on a Linux based DAQ computer.

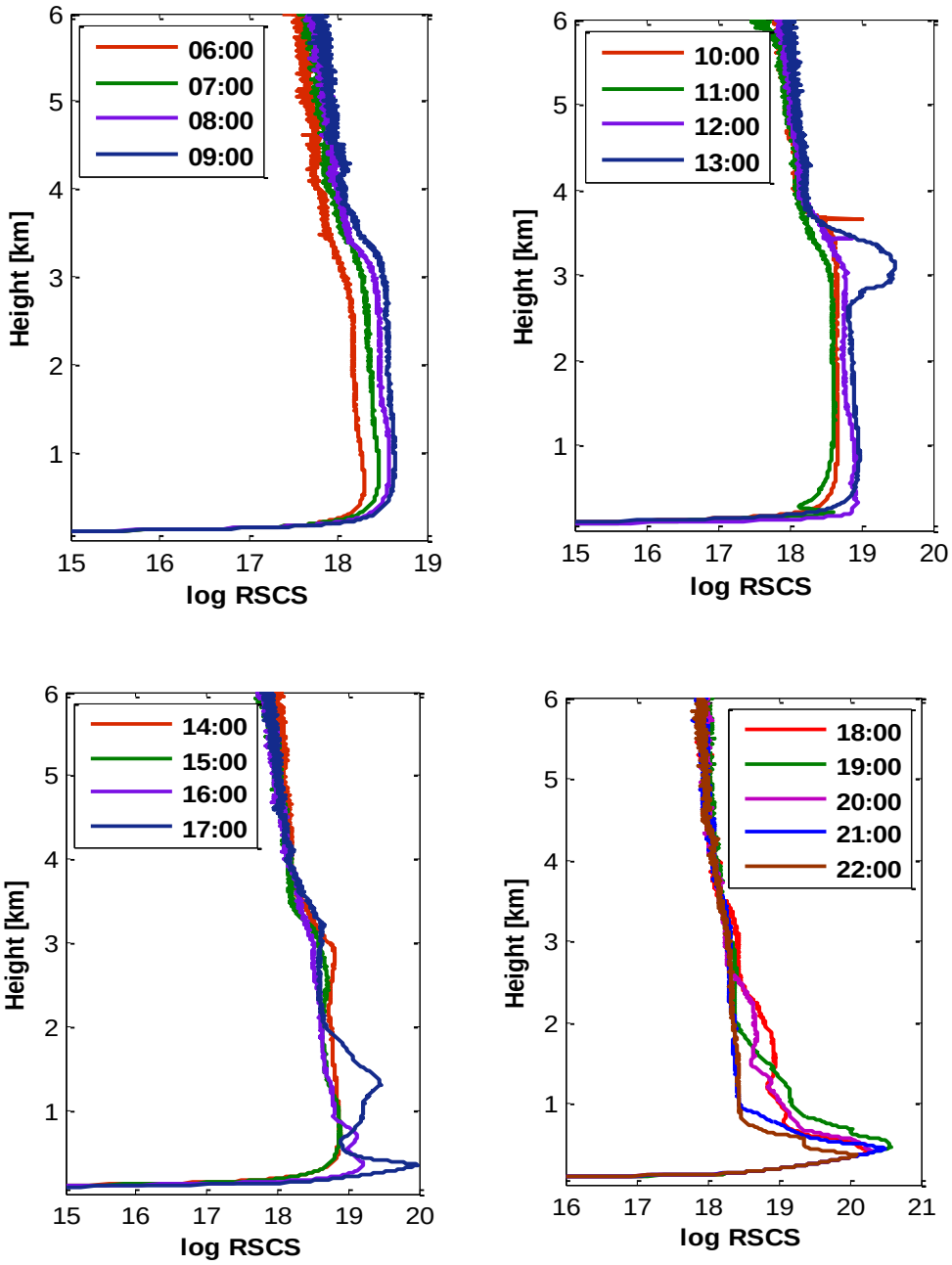

Figure 13: Time series of logarithm of range-squared signal profiles for 14 January 2012. Height is given relative to lidar site. In the morning, the aerosol concentration was low, and the atmosphere was stable. At noon, around 13:00, we detected a cloud at the height of 3 - 4 km. In the afternoon, and during the evening, the aerosol concentrations were high, with a maximum concentration at 19:00 at the height of 0.6 km.

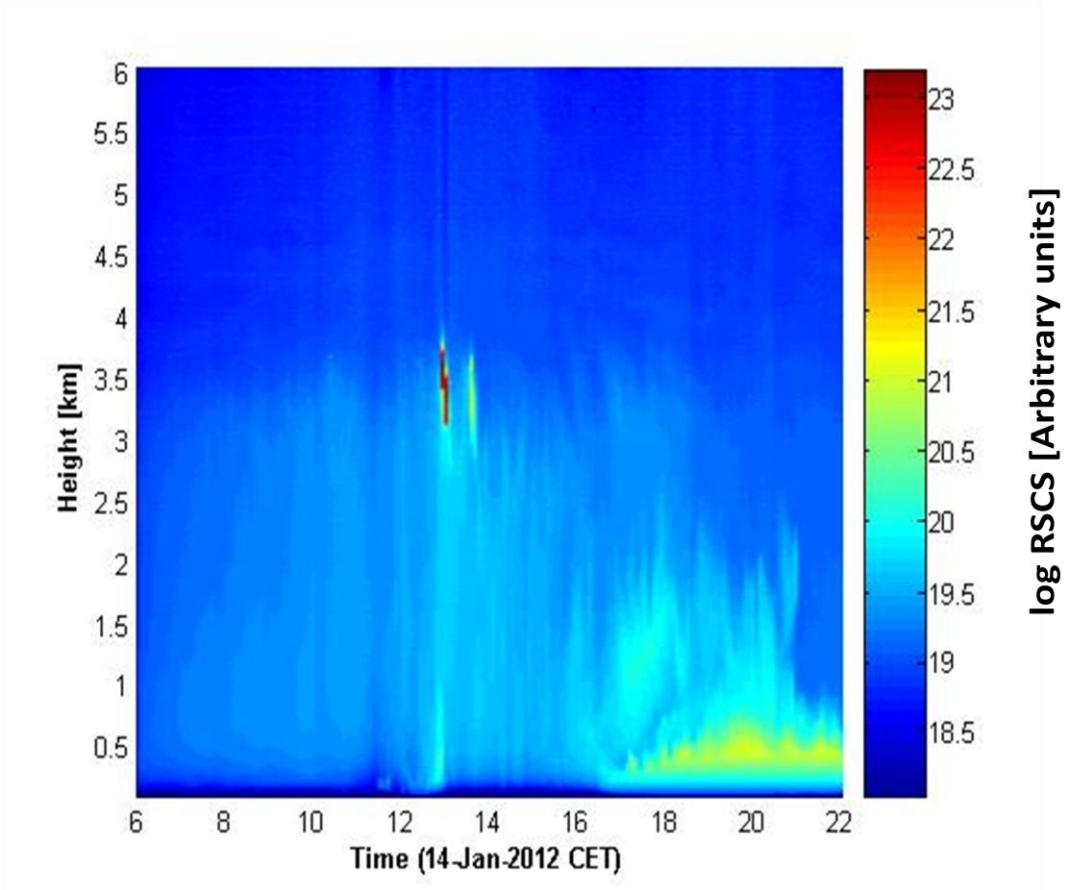

Figure 14: Time-Height-Indicator (THI) of logarithm of range-squared signal profiles for 14 January 2012. Height is given relative to altitude of the lidar site. THI diagram shows that in the morning the atmosphere was calm. At noon, there was a cloud detected at around 13:00 CET at the height of 3 – 4 km. After 17:00 CET, the atmosphere, the aerosol concentrations were high, and the maximum concentration was at around 19:00 CET at the height of 0.6 km.

4.1 Atmospheric extinction

In order to get quantitative information about daily variation aerosol concentrations lidar returns were transformed into atmospheric extinctions. Extinction coefficients were retrieved from the lidar return signals using Klett method [12], (Eq. 19). In the Klett method algorithm, aerosol extinction coefficient and backscatter coefficients are related by expression $\beta(r) = A\alpha(r)^k$, where *k* depends on the lidar wavelength and

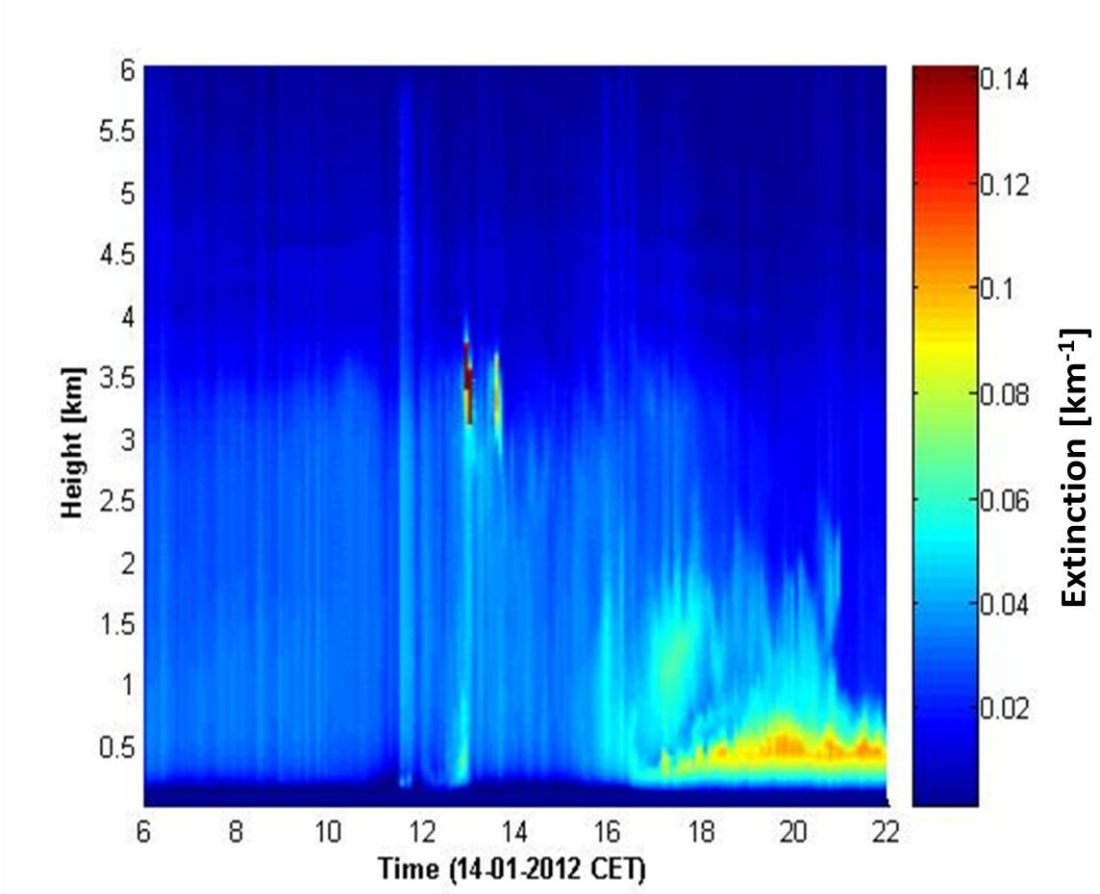

Figure 15: Time-Height-Indicator (THI) of atmospheric extinction for 14 January 2012. Height is given relative to altitude of the lidar site. THI diagram shows that in the morning the atmosphere was calm. There was no aerosol content. The elevated extinction values around 13:00 CET at the height of 3 – 4 km were caused by a passing cloud. In the afternoon aerosol concentrations gradually increased. Maximum extinction coefficient was found around 19:00 CET at the height of 0.6 km.

properties of the aerosols. Values of the exponent lie in the interval $0.67 \le k \le 1.0$. According to (Eq. 19), the aerosol extinction α_m at maximum detection range S_m can be written as $\alpha_m = LR \cdot \beta_m$, where LR is lidar ratio. For our measuring campaign, lidar ratio was assumed to be 50 [14]. The backscattering coefficient at maximum detection β_m was calculated according to U. S. Standard Atmosphere Model (1976) [15]. Using this technique, the extinction coefficients were calculated for the entire available dataset.

The time-height-indication (THI) diagram presenting the variation of atmospheric extinction is shown in Fig. 15. The diagram shows that in the morning atmospheric conditions were quite stable. At noon, passing cloud has been detected at 13:00 CET at height of 3 - 4 km, above the ABL. An aerosol layer started to develop after 17:00 CET, reaching a maximum concentration (α = 0.07 km^{-1}) at around 19:00 CET at the height of 0.6 km, within the ABL. Detailed information on the extinction values are graphically presented in the elevation profiles of extinction coefficients (Fig. 17).

In addition, we studied the variation of atmospheric extinction coefficient with time at fixed heights of 0.5 km, 1 km, 2 km, and 5 km. Figure 16 shows that there is almost no change in the extinction coefficient for the heights of 2 km and 5 km, which implies that they are above the ABL. For the heights of 0.5 km and 1 km distinct variation of atmospheric extinction is visible, which implies that they are within the ABL.

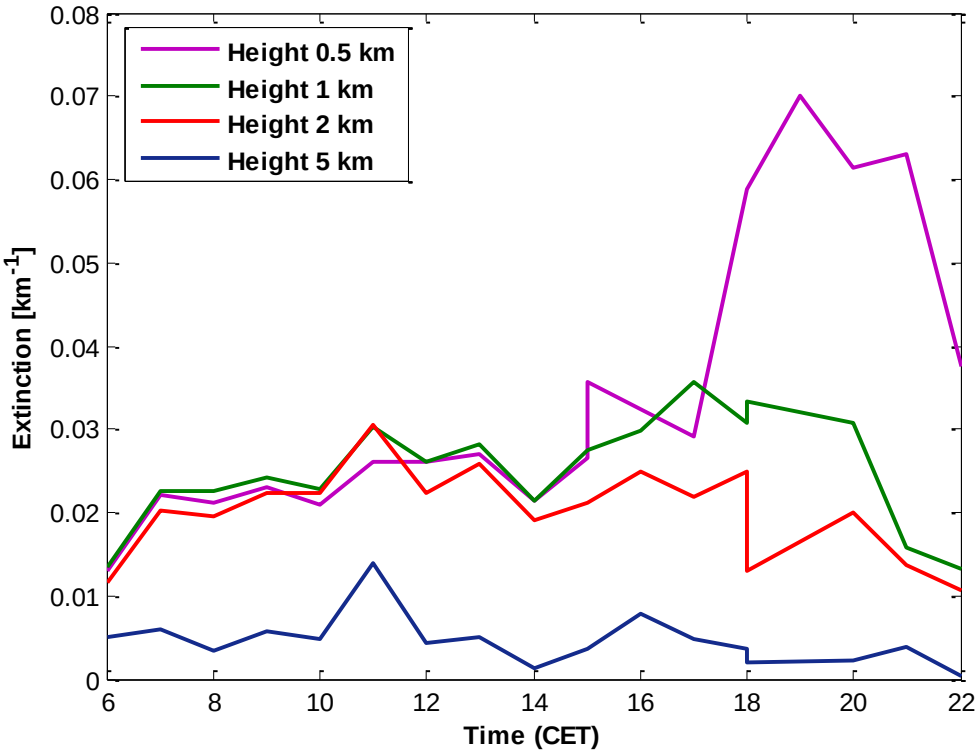

Figure 16: Variation of atmospheric extinction coefficients with time at various heights, relative to the lidar site. Time refers to CET. Atmospheric extinction is quite constant at the heights of 2 km and 5 km, they are outside of ABL. The decrease of the magnitude of the extinction pick with height furthermore implies that aerosols in the ABL originate from local-ground sources.

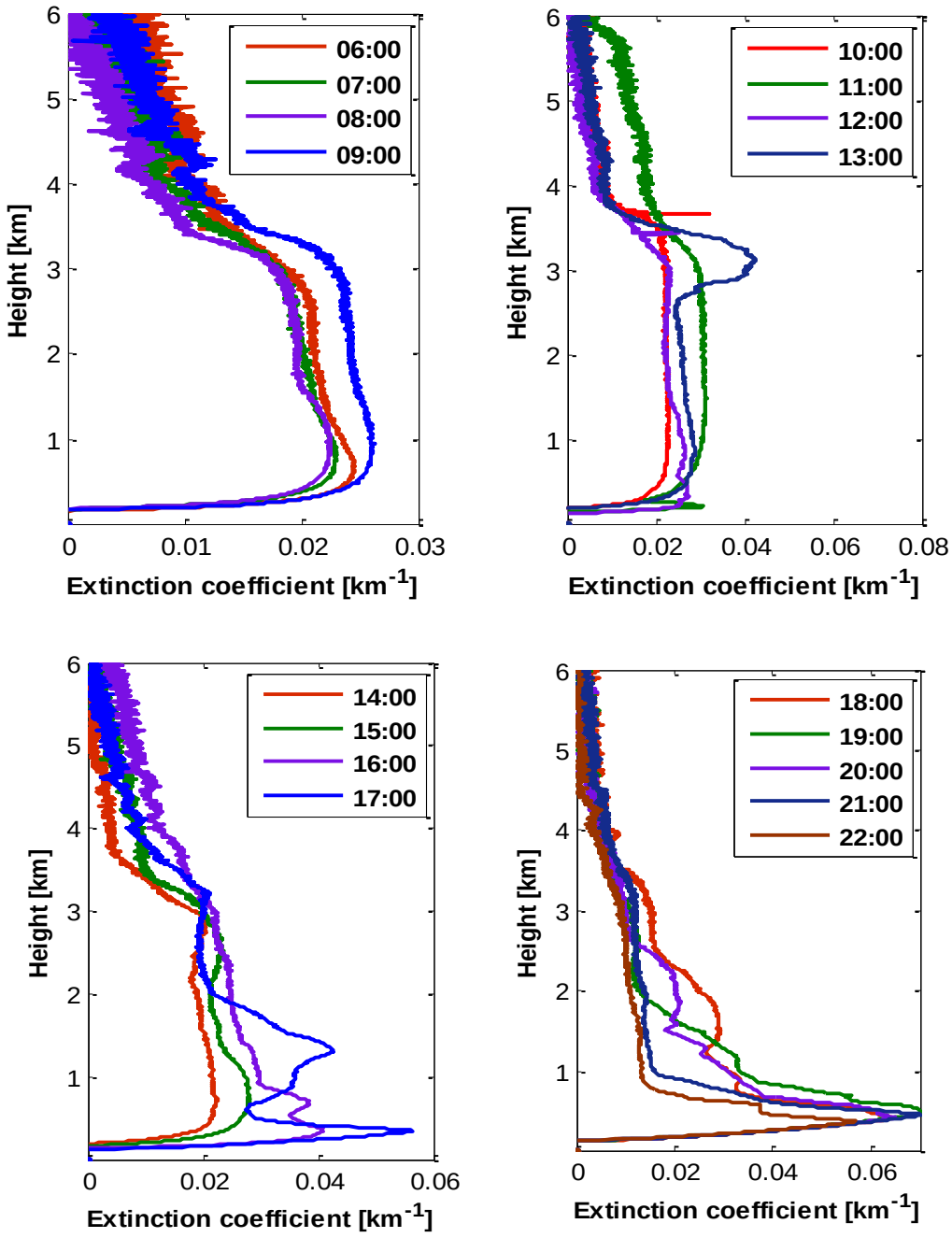

Figure 17: Time series of atmospheric extinction profiles on 14 January 2012. Height is given relative to lidar site. From the profiles, we can obtain that in the morning atmospheric conditions were stable. At noon, around 13:00 CET was detected cloud at the height of 3 – 4 km. In the afternoon, after 17:00 CET were developed more aerosol layers, with maximum concentration (α = 0.07 km^{-1}) at around 19:00 CET at the height of 0.6 km.

5. COMPARISON OF LIDAR AND GROUND-BASED MEAUSUREMENTS

To verify lidar measurements and to correlate the obtained atmospheric extinction coefficients to particle concentrations PM_{10} and NO_x gases, lidar results were compared to environmental and other meteorological data, which were collected 3 km from the lidar site by the Slovenian Environment Agency.

Figure 18: Air quality monitoring station by Slovenian Environment Agency located in Nova Gorica. The station continuously monitors wind speed and direction, temperature, relative humidity, air pressure, concentration of particles with size 10µm (PM_{10}) and NO_x gases.

The monitoring site is located in a commercial region of Nova Gorica (Fig. 18). Wind speed was measured at 10 m above the ground, temperature and relative humidity were measured at 2 m above the ground. The temporal evolution of these meteorological data (Fig. 19) shows that the atmosphere was very calm. The wind speed was very low, for most of the time only 0.5 m/s. Around 15:00 CET wind speed also increased to about 3.4 m/s due to convection. The highest value of air pressure was 1008 mb around 11:00 CET and the lowest was found to be 1005 mb around 15:00 CET. The concentration of PM_{10} particles and NO_x concentration reach pick values around 12:00 CET and 22:00 CET, and 10:00 CET and 20:00 CET, respectively, which was found to be strongly related to human activities.

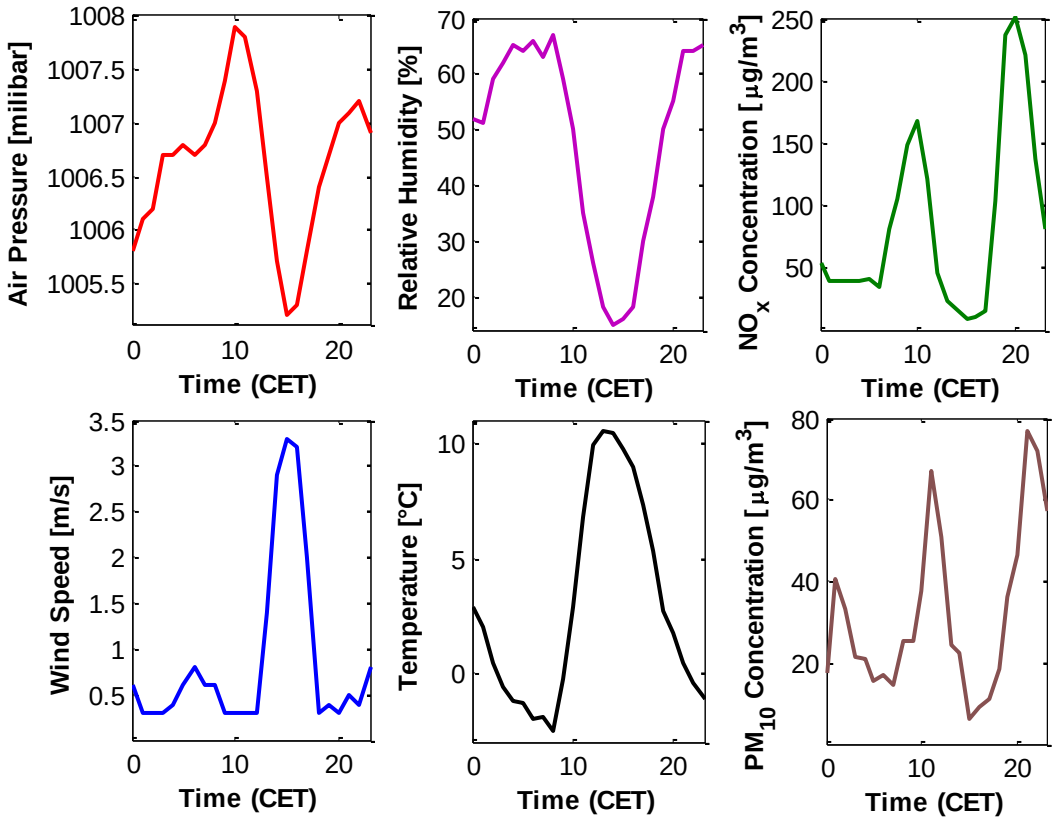

Figure 19: Meteorological data for Nova Gorica on 14 January 2012. Temporal evolution of PM_{10} and NO_x concentrations during the day. Wind speed was obtained at 10 m above the ground, temperature and relative humidity at 2 m above the ground.

From the Fig. 19 we can obtain that concentrations of PM_{10} particles and NO_x concentrations are in a good agreement. Both of them show high concentrations around

12:00 CET in the morning and 22:00 CET in the evening, and around 10:00 CET and 20:00 CET, respectively. These concentrations are expected to be highly correlated. In order to get information about correlation between them, we calculated the correlation coefficient. The correlation between them is linear, with a correlation coefficient of 0.61, (Fig. 21).

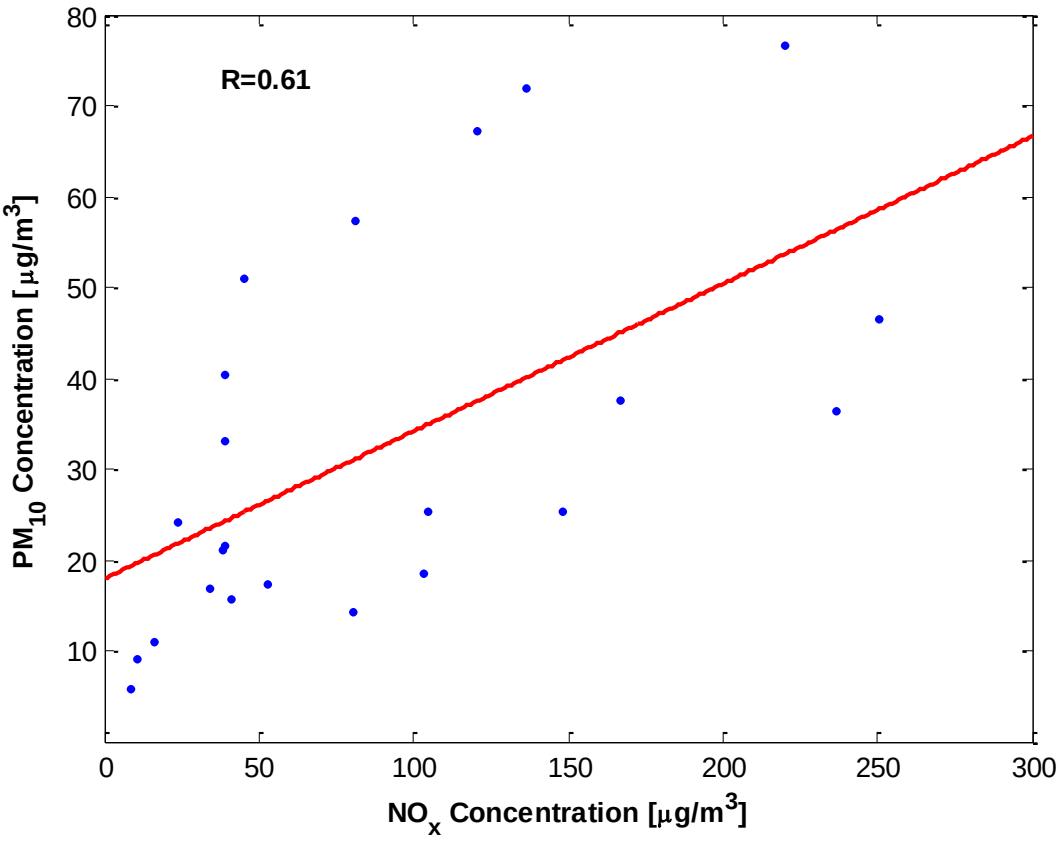

Figure 21: Correlation between concentrations of NO_x gases (c_{no}) with concentration of PM_{10} particles (c_{pm}) obtained from the ground-based measurements by the Slovenian Environment Agency. The correlation is found to be linear, $c_{pm} = 0.16207\ c_{no} + 18.004$, with a correlation coefficient of 0.61.

As the aerosol extinction (α) is a result of Mie scattering on particulate matter in the atmosphere, it is expected to be highly correlated to concentrations of PM_{10} particles and NO_x [10]. We found a correlation and calculated the correlation coefficient between them. The correlation between them is found to be linear. Correlation between

PM_{10} and extinction coefficient (α) is found to be 0.34, and correlation between NO_x and extinction coefficient (α) is 0.66, (Fig. 22).

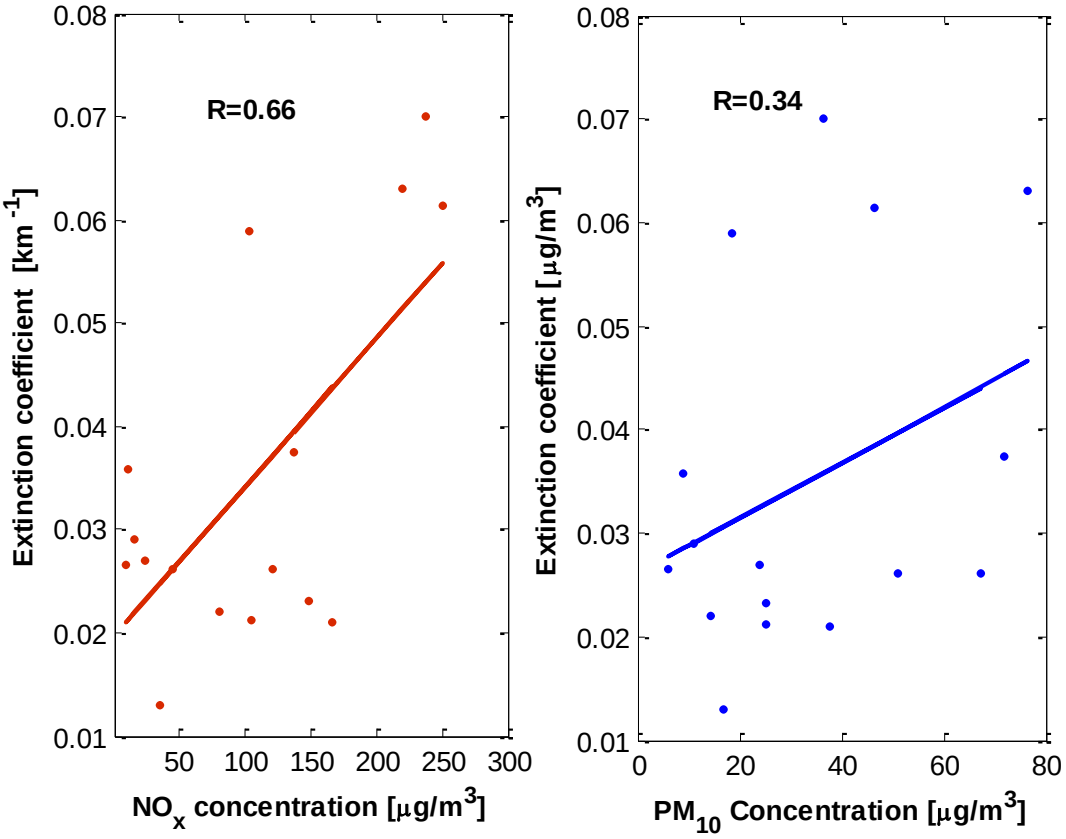

Figure 22: Left: correlation between concentrations of PM_{10} particles obtained from the Slovenian Environment Agency and extinction coefficient α retrieved from lidar-based measurements. The correlation is found to be linear, α =0.00014419 c_{pm} + 0.01972, with a correlation coefficient of 0.66. Right: correlation between concentrations of NO_x gases obtained from the Slovenian Environment Agency and extinction coefficient α retrieved from lidar-based measurements. The correlation is found to be linear, α =0.00014419 c_{no} + 0.01972, with a correlation coefficient of 0.34.

The trends of this data are in good agreement. This indicates that main sources of aerosols are from local origin. The major sources of uncertainties are expected to be the different location of the two measurements - PM_{10} and NO_x data and lidar measurements were performed at distance of 3 km.

5.1 Search for possible aerosol sources

The origin of air masses above Nova Gorica was investigated using **HY**brid **S**ingle-**P**article **L**angrangian **I**ntegrated **T**rajectory (**HYSPLIT)** model [16, 17]. Figure 20 (left) shows an example of the simulations of 96-h backward trajectories with 6-h temporal resolution for Nova Gorica on 14 January 2012 at 13:00 UTC. The end-point altitudes were 500, 1500 and 3000 m, considering that the height of the ABL in Europe is typically less than 2 km above the ground [2]. Simulations of backward air flow trajectories, which were made for the whole day, from 05:00 UTC to 21:00 UTC (Coordinated Universal Time), show that air masses originated predominantly from north and north-west regions and were expected to contain very low concentration of aerosols.

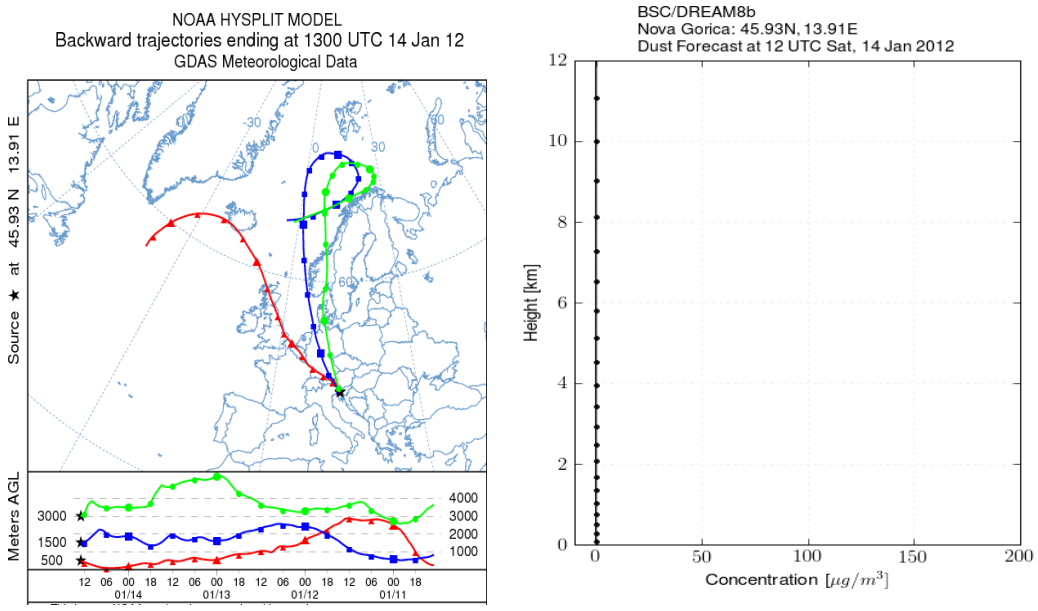

Figure 20: Example of backward air flow trajectories reaching Nova Gorica at 13:00 UTC at heights 500, 1500 and 3000 m for a 96-h time interval with 6-h temporal resolution obtained from HYSPLIT (left) and Saharan dust concentrations obtained from DREAM model for 14 January 2012 (right) for 14 January 2012.

In addition, we also checked the possibility of the presence of Saharan dust. **D**ust **RE**gional **A**tmospheric **M**odel (**DREAM**) is a model designed to simulate and/or predict the atmospheric cycle of mineral dust aerosol [16, 17]. From this model we can obtain the type of the aerosols detected by the lidar. Figure 20 (right) shows that there are no Saharan dust concentrations on 14 January 2012.

6. SUMMARY AND CONCLUSIONS

A measuring campaign was performed on 14 January 2012 in order to investigate daily aerosol concentrations in the atmosphere above Nova Gorica. As the detection tool we used the mobile lidar developed at Center for Atmospheric Research of the University of Nova Gorica. From the collected data we calculated extinction coefficient using the Klett method [12]. The retrieved extinction coefficient values were compared to concentrations of PM_{10} particles and NO_x gases, which are being routinely monitored by the Slovenian Environment Agency at the distance of 3 km from the lidar site. In order to identify the sources and the types of aerosols, we modeled the arrival trajectories of air masses above Nova Gorica using the HYSPLIT and DREAM models.

Aerosol extinction coefficient, obtained from the lidar data and concentrations of PM_{10} and NO_x, were found to be linearly correlated with correlation coefficient of 0.34 and 0.66, respectively. The concentrations of NO_x and PM_{10} were also found to be correlated with correlation coefficient of 0.61. Air flow trajectories modeled by the HYSPLIT model [16] showed that air masses during the lidar measurements originated from the Northern Atlantic arrived from the north and north-west and were thus expected to carry a very limited amount of aerosols. In addition, DREAM model [17] showed that during the measurements no Saharan dust was expected to appear above Nova Gorica.

From the combined data we can conclude that aerosols observed originated from local ground sources. Local traffic and human activities were found to play an important role in air pollution in Nova Gorica region.

BIBLIOGRAPHY

[1] M. Trošt: "*Zaznavanje Saharskega prahu v tropospheri*", Diplomsko delo, Univerza v Ljubljani, 2011.

[2] F. Gao, K. Bergant, A. Filipčič, B. Forte, D.-X. Xua, X.-Q. Song, S. Stanič, D. Veberič, M. Zavrtanik: "*Observation of the atmospheric boundary layer across land-sea transition zone using a scanning Mie lidar*", Journal of Quantitative Spectroscopy and Radiative Transfer, 112(2), 182-188, 2011.

[3] V. A. Kovalev,W. E. Eichinger: "*Elastic lidar. Theory, practice and analysis methods*", John Wiley and Sons, Inc., Hoboken, New Jersey, 2004.

[4] M. Čolović-Daul: "*Lidar sensing of aerosols and determination of their trajectories*", Master thesis, University of Nova Gorica, 2007.

[5] S. Christoph, B. Chuck, O. John, F. Grahan, G. Georg: "*Aerosols: Air & Quality*" : http://www.esrl.noaa.gov/research/themes/aerosols/pdf/AerosolIntro.pdf

[6] C. Weitkamp: "*Lidar, Range-Resolved optical Remote Sensing of the Atmosphere*", Springer series in optical science, New York, 2005.

[7] F. Gao: "*Study of process in atmospheric boundary layer over land-sea transition interface using scanning lidar*", Dissertation, University of Nova Gorica, 2012.

[8] T-Y. He, F. Gao, S. Stanič, D. Veberič, K. Bergant, A. Dolžan, and X.-Q. Song: *"Scanning Mobile Lidar for Aerosol Tracking and Biological Aerosol identification",* Proceeding of SPIE, 7832, 7832U, 2010.

[9] T.-Y. He, S. Stanič, W. Eichinger, B. Barnhart: "*Investigation of vertical aerosol distributions in the vicinity of Iowa city*", Proceeding of the 26th International Laser Radar Conference, Greece, 25-29 June 2012.

[10] T-Y. He, F. Gao, S. Stanič, D. Veberič, K. Bergant, X.-Q. Song and A. Dolžan, and: *"Tracking of urban aerosols using combined lidar-based remote sensing and ground-based measurements",* Atmospheric Measurement Techniques, 5, 891-900, 2012.

[11] M. Trošt: "*Detection of biological aerosols using induced fluorescence lidar*", Seminar, University of Ljubljana, 2008.

[12] J. D. Klett, "*Stable analytical inversion solution for processing lidar returns*", Applied Optics, 20(2), 211-220, 1981.

[13] J. H. Richter, H. G. Hughes, M.R. Paulson: "*Remote sensing of extinction using single-ended lidars"*, National Radio Science, 22, 1-5, 1992.

[14] A. Ansmann, U. Wandinger, M. Riebesell, C. Wietkamp, W. Michaelis: "*Independent measurement of extinction and backscatter profiles in cirrus clouds by using a combined Raman elastic backscatter -lidar*", Applied Optics, 31, 7113-7131, 1992.

[15] "*U. S. Standard atmosphere, 1976*", US Government Printing Office, Washington D.C., 1976.

[16] HYbrid Single-Particle Lagrangian Integrated Trajectory. http://www.arl.noaa.gov/HYSPLIT_info.php.

[17] M. Čolović-Daul, K. Bergant, B. Forte, A. Filipčič, F. Gao, M. Zavrtanik, S. Stanič: "*Study of air flow characteristics above Slovenia by cluster analysis and lidar detection of aerosols*", Internal report, 2009.

[18] Dust REgional Atmospheric Model. http://www.bec/es/projects/earthscience/DREAM.